BNL 39724

AN INTRODUCTION TO THE PHYSICS AND INSTRUMENTATION OF POSITRON EMISSION TOMOGRAPHY

BNL--39724

DE87 010041

G. W. Bennett

Brookhaven National Laboratory

Upton, NY 11973

INTRODUCTION

Positron emission tomography is a procedure which uses pharmaceuticals labeled with positron emitting radionuclides to examine regional functional performance in-vivo. It offers the best prospects for spatial resolution in emission tomography. The maturation of this field is due to the skills and industry of a dedicated cadre of chemists, engineers, pharmacists, physicians, and physicists.

Positron emitters may be characterized by chemical species, half-life, positron energy, and the presence of other emissions. The major cyclotron-produced nuclides used for PET are listed in Table I. They have relatively short half-lives and represent chemical species common in human body composition, making their implementation more straightforward than may be the case for other positron emitters. However, their major advantages are the practical range of lifetimes, low positron energies, and absence of other radiations. Their main drawback is that their short lifetimes, which minimize dose and permit sequential studies, require that the production accelerator be nearby.

A second class of positron emitters are the radionuclide daughters via beta decay of a longer lived parent nuclide. These generator produced isotopes have an effective shelf lifetime, for storage and transport, determined by the parent, while the eluate can have a half-life appropriate to medical imaging applications. Representative generator systems are listed in Table II (adapted from Yano, 1986).

Table I. Cyclotron Produced Radionuclides for PET

Radionuclide	Half-Life (Min)	β+ Decay %	E_{MAX} (MeV)	Daughter

Brookhaven National Laboratory

Upton, NY 11973

INTRODUCTION

Positron emission tomography is a procedure which uses pharmaceuticals labeled with positron emitting radionuclides to examine regional functional performance in-vivo. It offers the best prospects for spatial resolution in emission tomography. The maturation of this field is due to the skills and industry of a dedicated cadre of chemists, engineers, pharmacists, physicians, and physicists.

Positron emitters may be characterized by chemical species, half-life, positron energy, and the presence of other emissions. The major cyclotron-produced nuclides used for PET are listed in Table I. They have relatively short half-lives and represent chemical species common in human body composition, making their implementation more straightforward than may be the case for other positron emitters. However, their major advantages are the practical range of lifetimes, low positron energies, and absence of other radiations. Their main drawback is that their short lifetimes, which minimize dose and permit sequential studies, require that the production accelerator be nearby.

A second class of positron emitters are the radionuclide daughters via beta decay of a longer lived parent nuclide. These generator produced isotopes have an effective shelf lifetime, for storage and transport, determined by the parent, while the eluate can have a half-life appropriate to medical imaging applications. Representative generator systems are listed in Table II (adapted from Yano, 1986).

Table I. Cyclotron Produced Radionuclides for PET

Radionuclide	Half-Life (Min)	β+ Decay %	E_{MAX} (MeV)	Daughter
Carbon-11	20.4	99.8	0.96	^{11}B, stable
Nitrogen-13	9.96	100	1.20	^{13}C, stable
Oxygen-15	2.07	99.9	1.73	^{15}N, stable
Fluorine-18	109.7	96.9	0.63	^{18}O, stable

Table II. Characteristics of Positron Emitter Generators

Parent/ Daughter	Parent $T_{1/2}$	Daughter $T_{1/2}$	Daughter Emissions		
			Mode (%)	E_γ(%) keV	$E_{\beta+}$ MAX MeV
$^{44}Ti/^{44}Sc$	47 years	3.93 hr	β^+(95)	511 (190)	1.47
			EC (5)	1,159 (100)	
$^{52}Fe/^{52m}Mn$	8.28 hr	21.4 min	β^+(96)	511 (193)	2.63
			IT (2)	1,435 (98)	
$^{62}Zn/^{62}Cu$	9.26 hr	9.73 min	β^+(98)	511 (196)	1.31
			EC (2)		
$^{68}Ge/^{68}Ga$	288 days	68.1 min	β^+(90)	511 (178)	1.90
			EC (10)	1,077 (3)	
$^{72}Se/^{72}As$	8.4 days	26.0 hr	β^+(77)	511 (154)	2.50
			EC (23)	834 (80)	
$^{82}Sr/^{82}Rb$	25.0 days	1.25 min	β^+(96)	511 (192)	3.35
			EC (4)	776 (14)	
$^{118}Te/^{118}Sb$	6.0 days	3.5 min	β^+(75)	511 (150)	2.67
			EC (22)	1.23 (3)	
$^{122}Xe/^{122}I$	20.1 hr	3.6 min	β^+(77)	511 (154)	3.12
			EC (23)	564 (21)	
$^{128}Ba/^{128}Cs$	2.43 days	3.6 min	β^+(61)	511 (122)	2.89
			EC (39)	443 (22)	

It is worth noting that in general the maximum positron energy and the frequency of other emissions is greater for these generator produced isotopes than is the case for the "classic", cyclotron produced nuclides of Table I.

Generator Kinematics

Consider a system consisting of a parent nuclide (P) and a daughter product (D). Assuming that initially (t = 0) none of the daughter is present, the daughter activity varies with time as

$$A_D(t) = A_P(0)\frac{T_P}{T_P - T_D}\left[\exp(-t/\tau_P) - \exp(t/\tau_D)\right]$$

where τ indicates mean life time, T indicates half life.

If the lifetime of the parent is much greater than that of the daughter, and if the change in parent activity is negligible during the period of interest, then the daughter activity simplifies to

$$A_D(t) = A_P\left[1 - \exp(-t/\tau_D)\right]$$

that is, the daughter "charges up" to the same activity as the parent.

If the parent lifetime is greater than that of the daughter, and parent activity change is significant during the period of interest, the daughter activity increases from zero, attains a maximum value at

$$t_m = \frac{\tau_P \tau_D}{\tau_P - \tau_D} \ln(\tau_P/\tau_D)$$

then decreases, with an activity determined by the parent's lifetime. During this equilibrium the ratio of daughter to parent activity becomes

$$A_D/A_P = \frac{T_P}{T_P - T_D}$$

thus the product activity exceeds that of the parent!

Positron Interactions

Note that beta decay is a three body process where the recoiling nucleus, the positron (in this case) and a neutrino are emitted. The neutrino is uncharged, has a minute or zero mass, and can carry away some of the energy available in the decay process, but is undetectable with PET instrumentation. As a consequence the energy available for the positron is variable. A representative positron energy distribution is shown in Fig. 1.

The positron, after emission, dissipates its kinetic energy by interaction with the charged particles, principally electrons, in its path, traveling a distance from its emission site depending on its initial energy and on the (electron) density of the medium.

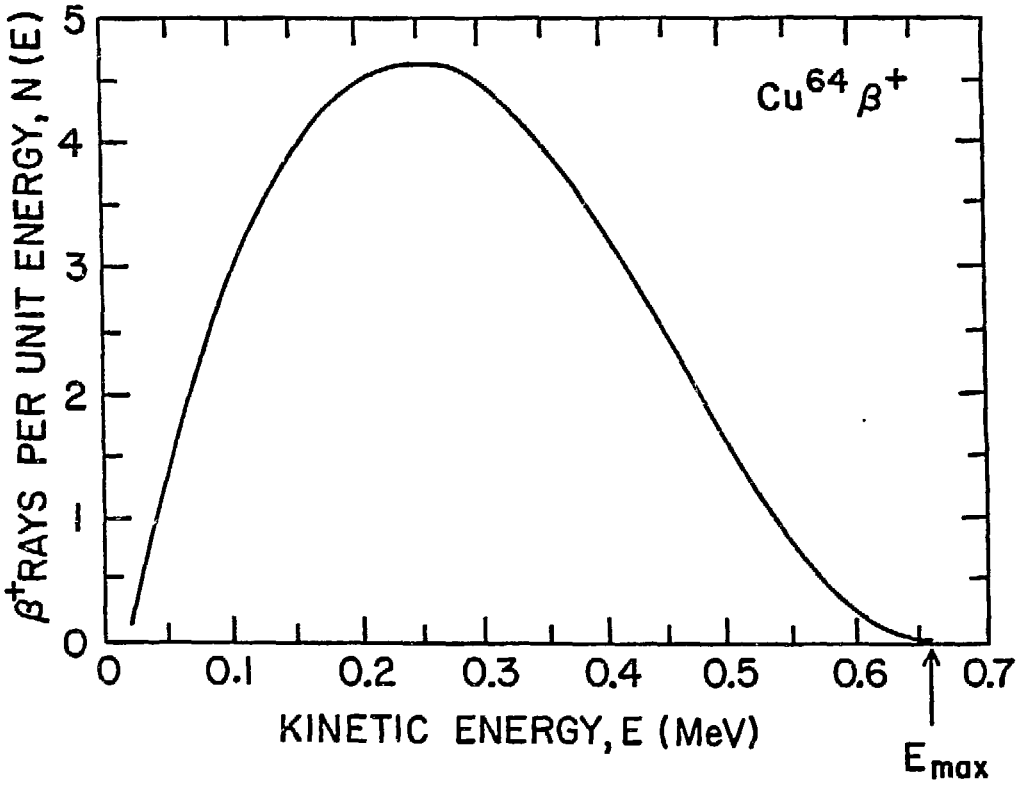

The positron is an anti-electron. It is a stable particle having the same mass as the electron, 511 KeV, but is oppositely charged. The interaction of matter and antimatter, termed annihilation, results in conversion of the original particle and antiparticle into electromagnetic radiation. The result is the appearance, generally, of two gamma rays, each of 511 KeV, termed annihilation photons or quanta. Although approximately 10% of the positrons interact "in flight", the balance annihilate at rest.

The simplistic, or zero order approximation to positron annihilation is that the two gamma rays are colinear and oppositely directed, emerging from the decaying nucleus (Fig. 2). A more realistic scheme allows that the gamma rays may originate from a site millimeters away from the decaying nucleus because of the initial kinetic energy of the positron; in addition, the gamma rays are not colinear (Fig. 3). That is, the positron transfers its kinetic energy to the electrons in its path by scattering, until it can form a "positronium" system with an electron. The two particles rotate about their mutual center of mass (which is not stationary because of thermal energy) descending through quantized energy levels until annihilation. Nearly all annihilation quanta occur in pairs but a minute fraction of the annihilations produces 3 quanta instead of two.

The positrons are emitted isotropically so that the finite "range" of these particles results in a blurring of the image. One tactic used in autoradography to reduce this effect, and proposed for PET, (Iida et al., 1986) is the introduction of an intense uniform magnetic field. The charged positrons tend to spiral about the magnetic field lines. The component of initial positron velocity parallel to the magnetic field is unaffected. The other two velocity components, in a plane perpendicular to the magnetic field, produce a force resulting in a circular orbit in that plane, where the orbit radius is smaller as the magnetic field strength is increased. The combination of linear and circular motions produces the spiral motion, reducing the blurring in all but the one dimension in the field direction.

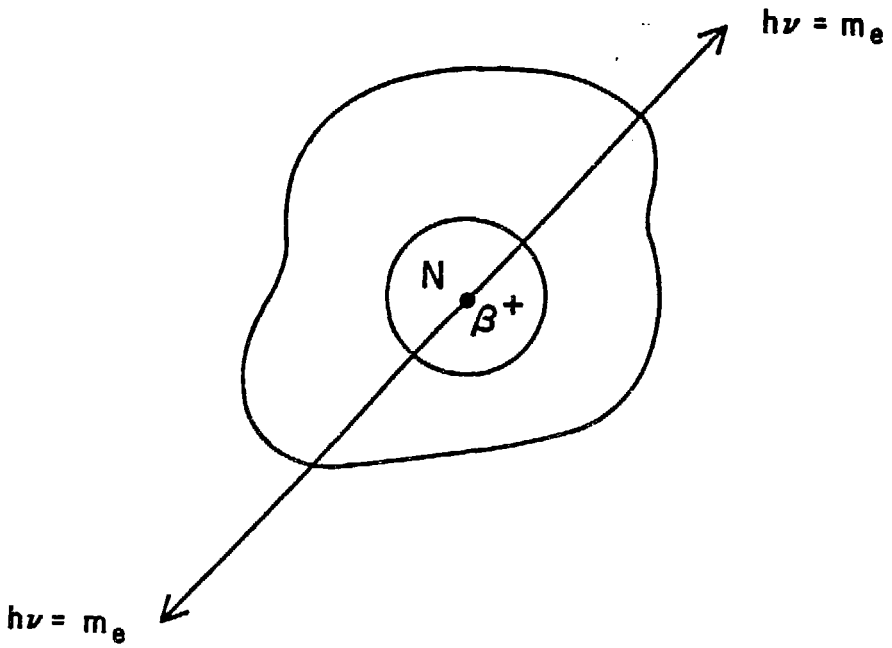

Fig. 2. Naive but workable view of positron emission and annihilation.

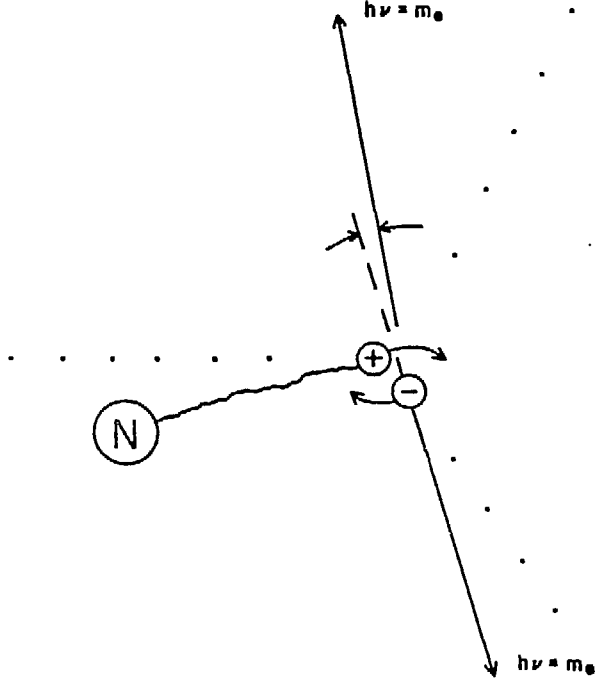

Fig. 3. A more accurate view of positron emission depicts the positron removed from the nucleus before annihilating, and the annihilation photons as not colinear.

The thermal motion of the positronium center of mass produces the non-colinearity of the annihilation photon. The departure from 180° is approximately 1/3° at room temperature.

The positron itself thus passes from consideration, replaced by a pair of annihilation photons, the particles which uniquely identify and point to a positron.

Gamma Ray Interactions

The interaction of gamma rays in matter is quite different from that of charged particles such as positrons. The positrons gradually lose their kinetic energy through a large number of small energy transfer interactions with other charged particles – atomic electrons. Neutral particles, however, interact but once, and may penetrate matter a vast number of atomic dimensions without absorption or scattering. Because of this process of "interacting at a point", a fixed fraction of a beam of photons is attenuated for each successive unit thickness of absorber traversed by the particles. The interaction is essentially probabilistic and leads to the exponential absorption law for a beam of such particles.

$$N(x) = N(0)\exp(-ux)$$

where N(0) is the incident flux, N(x) the flux at depth x, and u is the total linear attenuation coefficient.

Gammas with energy less than 1.02 MeV can interact only through the photo-electric effect, where the photon is absorbed and its energy transferred to an atomic electron, or through the quasi elastic collision process, Compton scattering. In this mode some of the original gamma's energy is transferred to an atomic electron, and a gamma ray of reduced energy emerges at an angle to the original trajectory. Using E_0

for the original energy, E for the final gamma energy, ϕ for the photon deflection angle, T for the electron energy, and m for the rest mass energy of the electron, the Compton Scattering relations are

$$E = E_0 \Big/ \left[1 + \frac{E_0}{m} (1 - \cos\phi) \right]$$

$$T = E_0 - E$$

for annihilation gammas $E_0 = m = 511$ KeV, therefore,

$$E = \frac{m}{2 - \cos\phi} .$$

However, there is an upper limit to the energy which the electron can absorb from a photon,

$$T_{max} = E_0 \Big/ \left[1 + \frac{m}{2E_0} \right]$$

corresponding to $\phi = 180°$, backscattering of the gamma. For annihilation radiation T_{max} is 2/3 E_0 or nearly 341 KeV. The minimum electron energy is zero.

It is worth noting that the total attenuation coefficient is the sum of absorption (photo electric) and scattering components. The photoelectric coefficient varies as E^m Z^n where Z is the atomic number of the material traversed; n ranges from 4 to 4.6, the energy exponent is usually given the value –3. The scattering coefficient varies directly as Z and decreases monotonically with photon energy. These will be useful in later discussions of detector materials, and attenuation.

Detectors

Positron emission tomography detectors operate by detecting electrons. Positrons have too little energy and range to exit the body; the annihilation gamma pairs have a high probability of exiting the body and intersecting a detector, and within the detector the electrons produced in absorption or scattering of the gamma ray are the medium for signal production.

The material used in detectors and the geometry employed are useful to characterize PET systems. The operation of the various systems are compared by means of performance parameters.

The primary parameters used to classify detectors are resolution (spatial, spectral and temporal), non-linearity (spatial and spectral) and sensitivity. Resolution is defined as the ability to distinguish nearby elements in the scene. Spatial resolution is then the minimum separation between two "points" in the field which appear distinct. In practice, the resolution is defined operationally as the full width at half maximum (FWHM) for a "point" source. Point here means much less than the resulting measured

resolution. The spectral resolution is similarly measured as the FWHM for a narrow (or "line") energy emission. Temporal resolution is limited by mechanical motion (the time to completely sample the field of view), or by statistics for a system which is stationary. Non-linearity is evidenced by the departure of the image spatial distribution from a precise mapping of the object distribution; straight lines in the object do not appear straight in the image. Spectral non-linearity is the apparent change in energy and energy resolution for a uniform monochromatic source viewed in different regions in the image. Sensitivity is usually defined as the detected count rate per unit activity per unit volume in a 20-cm diameter source uniformly distributed. The two components of sensitivity are geometric, relating to the solid angle of the detector elements subtended at the source point, and intrinsic, the fraction of events detected per photon incident on a detector element.

What properties are desirable in a detector for 511 keV gamma rays? Since the essential processes are electronic interactions, high density increases the probability of electron interactions. Obviously, the photo-electric interaction is preferable to Compton scattering in its ability to differentiate an annihilation photon from one that has scattered in tissue. Since the probability of photo-effect increases strongly with atomic number, the detector should have high Z.

The archetype detector is a scintillator mounted on a photomultiplier tube. In a scintillator, the electron produced by a gamma ray interaction produces photons in the visible range. These are conducted to the photomultiplier which converts the low energy photons into electrons, then amplifies these by many orders of magnitude. The overall process is linear. The energy of the initial gamma ray is proportional to the number of electrons produced and the charge output of the tube. Properties of typical scintillation materials are listed in Table III.

Table III. Scintillator Characteristics

Material	Percent Efficiency Rel. to NaI(Tl)	Decay Constant (μsec)	Wavelength (peak)	Index of Refraction	Density (g/cm^3)	Hydroscopic
NaI(Tl)	100	.23	410	1.85	3.67	Yes
CsF	5	.005	390	1.48	4.11	Yes
CsI(Tl)	45	1	565	1.8	4.51	Yes
CsI(Na)	85	.63	420	1.84	4.51	Yes
$Bi_4Ge_3O_{12}$ (BGO)	8	.3	480	2.15	7.13	No
$CdWO_4$	18	5	530	2.2	7.9	No
CaF_2(Eu)	50	.94	435	1.44	3.18	No
LiI(Eu)	35	1.4	485	1.96	4.08	Yes
BaF_2	10	.63*	310	1.49	4.88	No
Ce:Gd_2SiO_5 (GSO)	17	.06	430		6.71	No
Plastic	30	.002-.02	~400	~1.6	1.05	No

*Fast decay component at 220 nm is 700 ps. 80% of light is emitted in slow component. 20% is emitted in the fast component.

The concluding remark regarding the prototype detector is that it involves a second such detector, on the opposite side of the source, in coincidence (Fig. 4). The simultaneous detection of two annihilation photons registers the existence of a positron, and a line between the two detection sites localizes the nucleus which produced the positron. This detector pair has a sensitivity distribution measured by moving a point source through the intervening space with the detection rate at each point plotted as shown in Fig. 5. The equivalent figure for a single, collimated detector is seen in Fig. 6. It should be clear why the detector pair is said to exhibit "electronic collimation" and why PET is potentially superior to single photon tomography in resolution and sensitivity.

Positron scanners were commercially available in the early 1960s. A pair of detectors were mounted to a rectilinear scanning apparatus; the output device was a pen-plotter with the position of the pen related to the position of the detectors and the number of pen contacts proportional to the local signal intensity. A scanner of that era and a representative scan are shown in Fig. 7 (Aranow, 1962).

The standard PET geometry is a ring of scintillation detectors surrounding the source distribution (Fig. 8). Each detector is linked via a coincidence circuit to a number of detectors on the opposite side. Note that as the number of diametrically opposed detector elements in coincidence are increased, the sensitive area is increased,

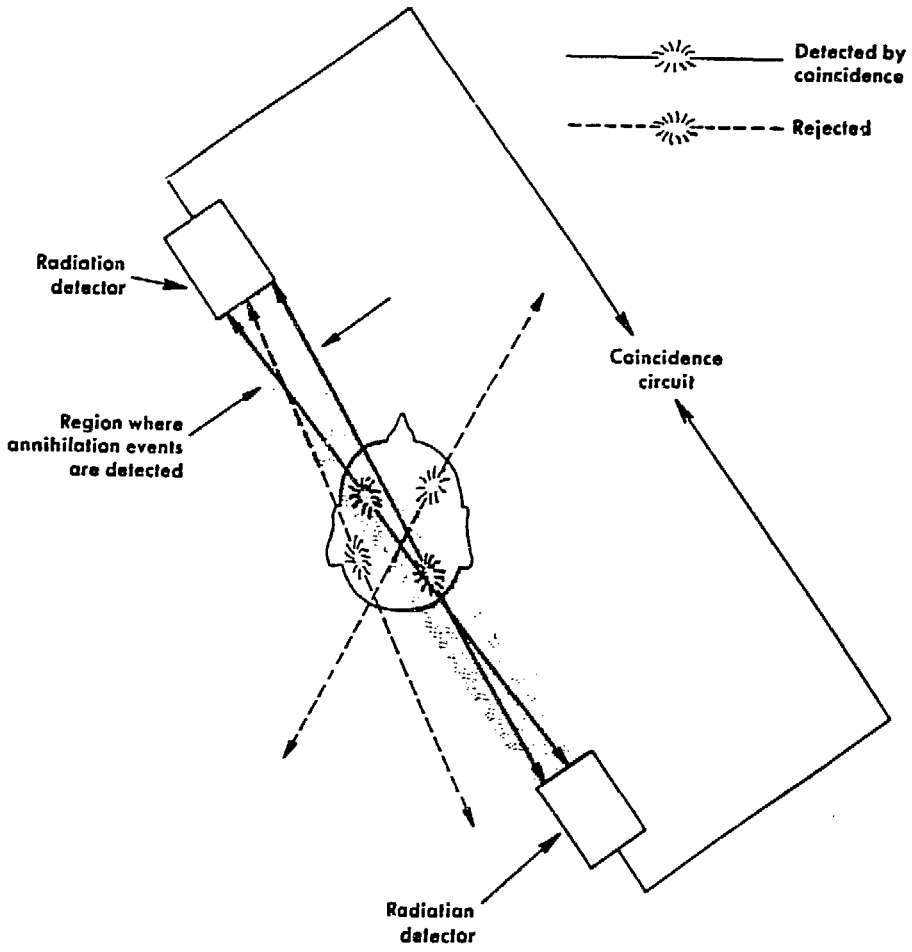

Fig. 4. A model positron detector consists of two photon detectors in coincidence (from Ter-Pogossian 1981).

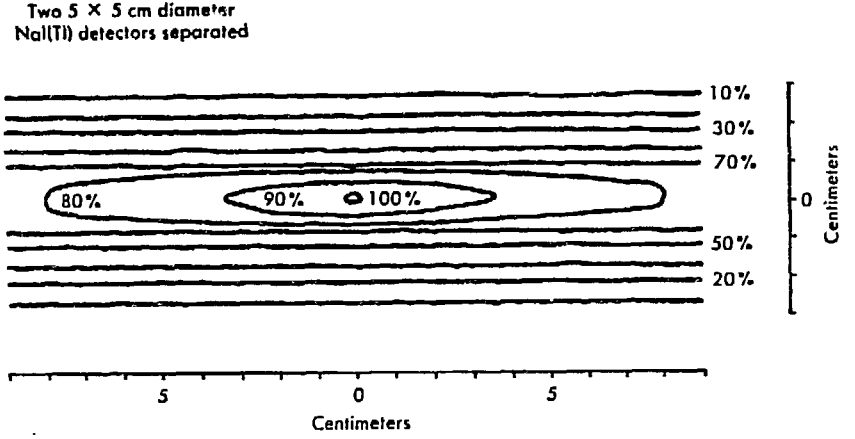

Fig. 5. Sensistivity distribution for two 5 cm diameter NaI (Tl) detectors in coincidence separated by 60 cm (from Ter-Pogossian 1981).

but the oblique rays have a reduced efficiency and an increased rate of cross talk, where the photons can scatter into neighboring detectors with increased detection probability.

The variety of geometric variation in PET detectors is manifold (Fig. 9) (from Budinger, 1978). Adjoining ring structures define a sensitive volume, often allowing coincidence signals between different rings, thus increasing the geometric efficiency at the penalty of non-uniform axial sensitivity. The ultimate geometric efficiency is offered by a distribution of detector elements completely surrounding the patient. A close approximation to this geometry (which has been proposed) is a truncated ellipsoid which nearly encloses the patient.

Other geometries include hexagonal arrays and planar detectors. A successful early model was the PETT III (Fig. 9i) consisting of 6 banks with 8 NaI detectors in each. Each detector in each bank could signal a coincidence with each of the 8 detectors in the diametrally opposed bank. The banks translated in 6 steps to sample the space between detectors, rotated one-twentieth (3 degrees) of the angular interval between banks, repeating the translational sampling after each rotation. Only one plane was sampled; the minimum scan duration was two minutes. The PETT III is soon to be installed at the Smithsonian Institute. A more modern system such as the PETT VI consists of 4 rings, each containing 72 detectors of CsF 20 mm × 24 mm ×

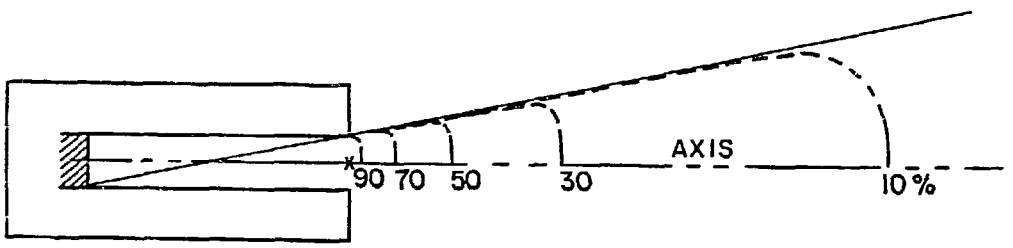

Fig. 6. Sensitivity distribution for a single scintillation detector having a cylindrical collimator with length 5 times its diameter. 100% sensitivity is chosen at the center of the collimator aperature.

Fig. 7a. Commercial positron brain scanner unit, 1962.

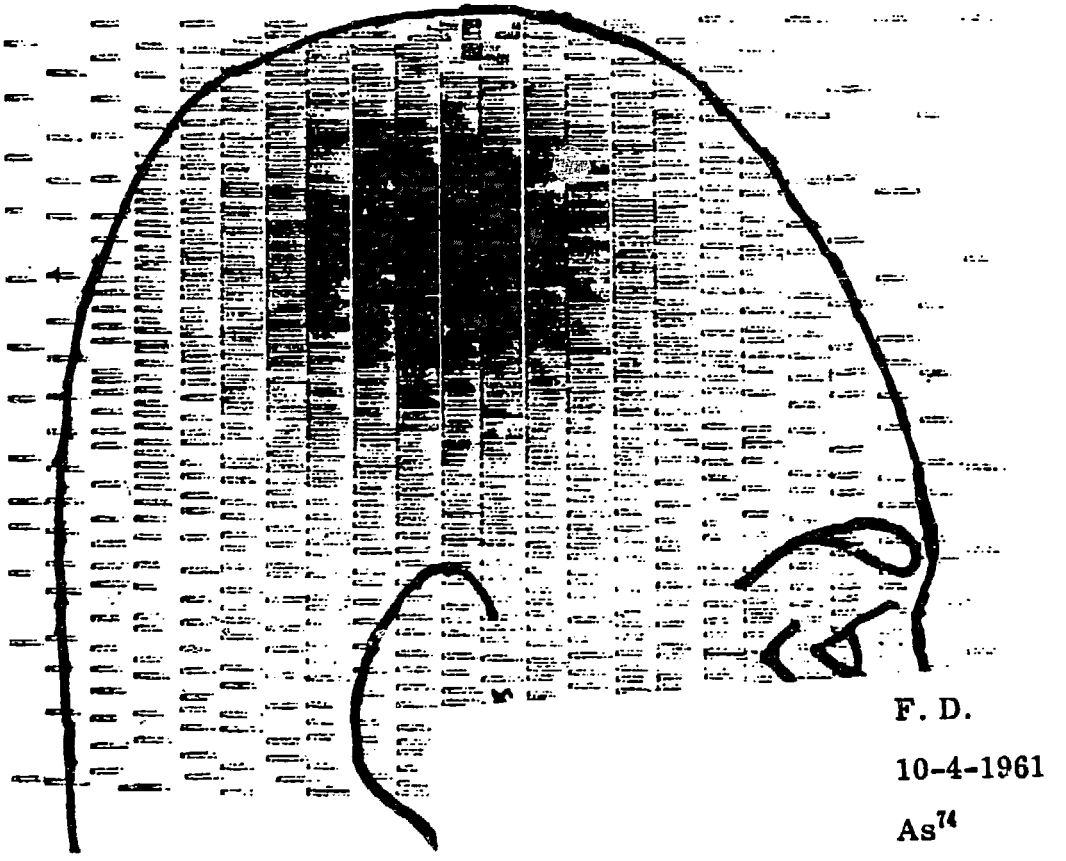

Fig. 7b. Representative brain scanner output.

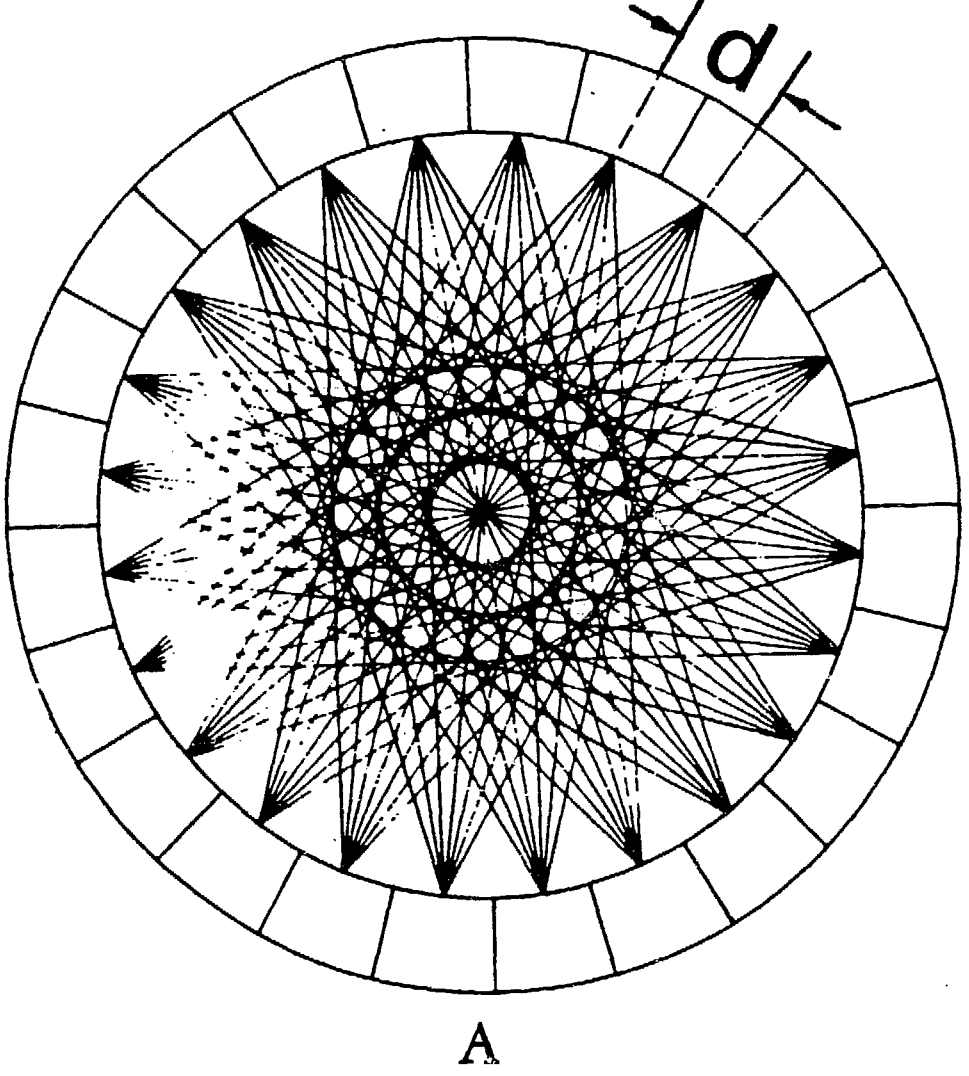

Fig. 8. Model positron emission tomography ring detector geometry (from Derenzo et al., 1981).

65 mm long. Coincidences between elements in adjacent rings produces 7 effective planes. Spatial sampling is accomplished by orbiting or wobbling the axis of the device in a small circle. The time for one cycle of motion is 1 second.

A scintillation camera is a single large crystal viewed by an array of photomultiplier tubes. Signals from the tubes go to summing amplifiers via approprately weighted resistors. Position signals are produced proportional to the centroid of the light in the crystal. Planar detectors such as scintillation cameras have been used in coincident pairs for PET. Large geometric efficiency results, but overall performance is poor. Since scintillation cameras are designed for optimal performance with Technetium 99m (140 KeV gamma) the crystals are too thin for good efficiency with annihilation radiation.

The concept of scintillation camera design has been applied (Burnham, et al., 1982) in one dimension to produce a ring scanner with the characteristics of a single crystal. The standard ring system design requires one phototube per crystal, and the

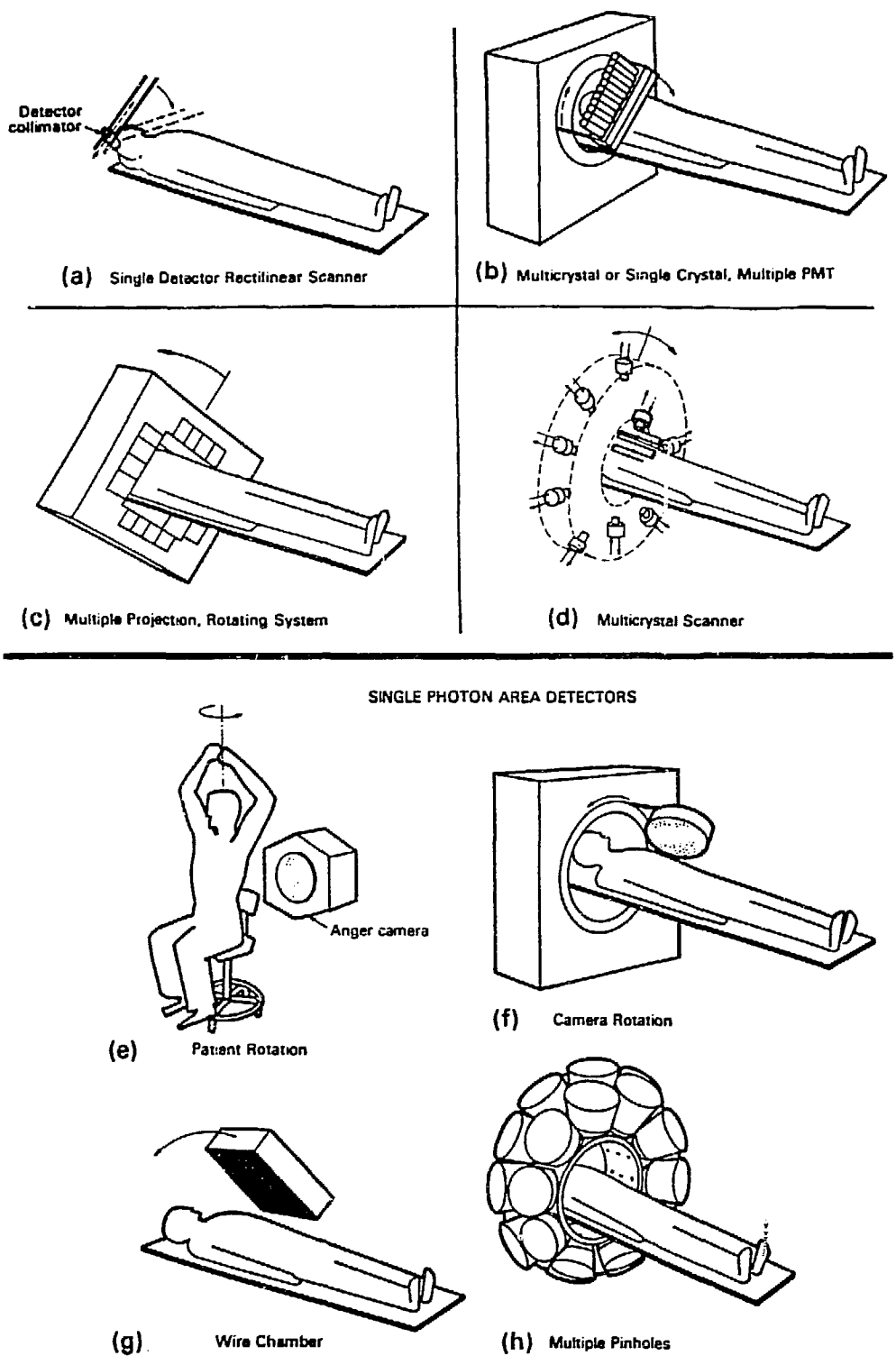

Fig. 9. Various PET geometries.

resolution is determined by the crystal size (and spacing). The application of the gamma camera principle affords a reduction in the number of photomultiplier tubes and associated circuits without degrading performance. Measured resolution in reconstructions is of the order of 5 mm for a detector with 46 cm internal diameter.

POSITRON SINGLE SECTION DEVICES

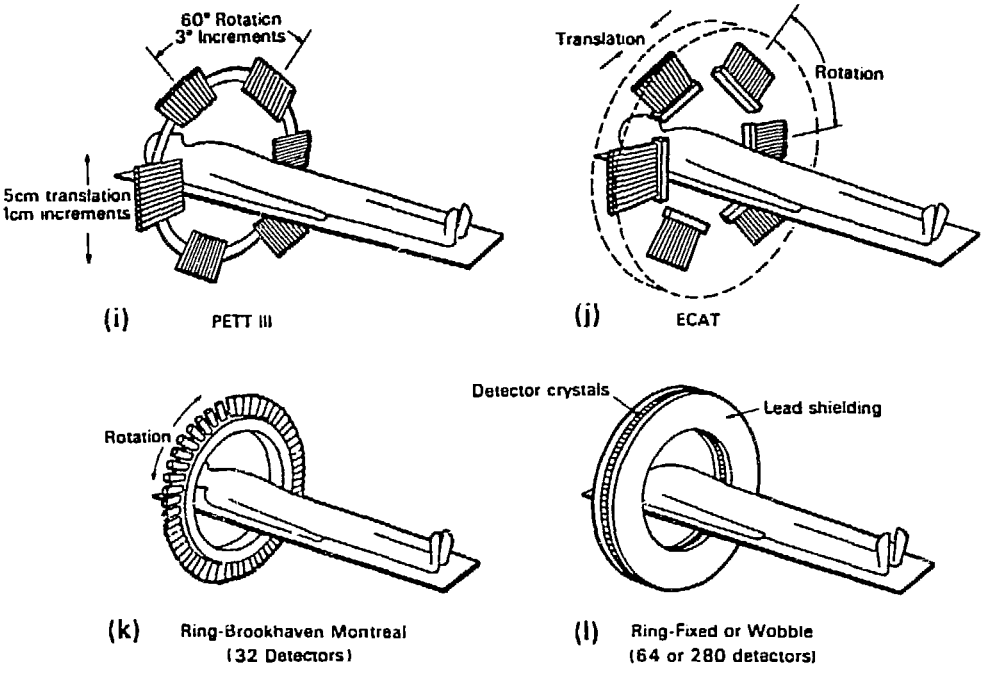

POSITRON AREA DETECTORS

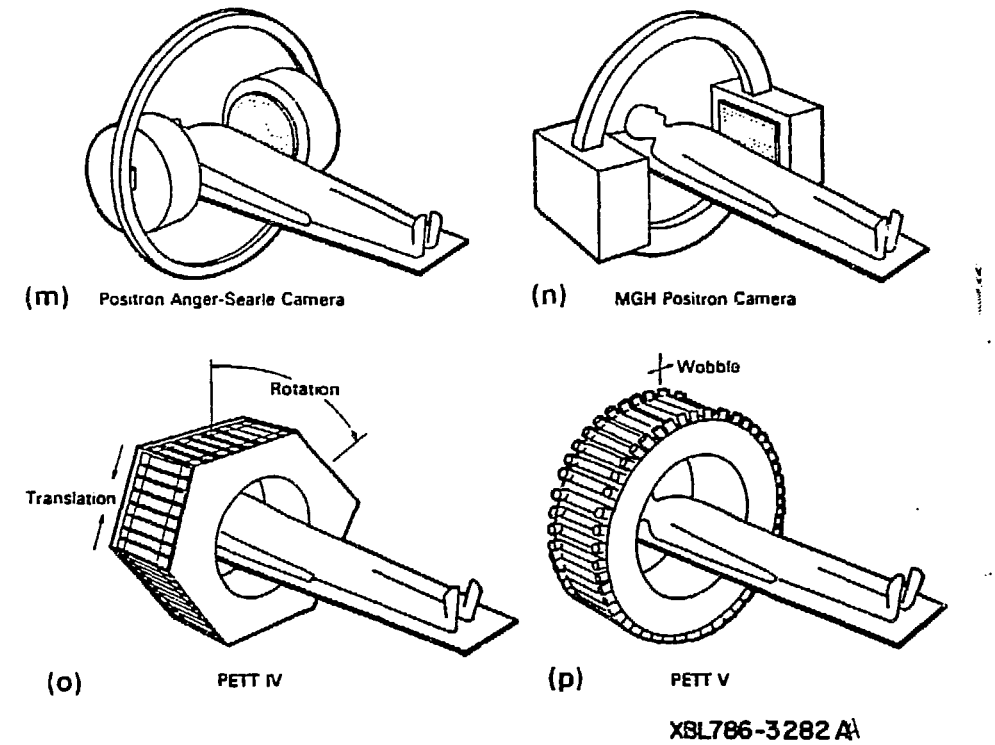

XBL786-3282 A

The gamma camera concept in two dimensions has been adapted for a hexagonal PET (Karp et al., 1986). Each of the six sides of the detector is a slab of NaI 110 mm wide, 470 mm long, and 25 mm thick, coupled to a two-dimensional array of 30 square phototubes (50 mm × 50 mm), the outputs of each of which are digitized directly. The spatial coordinates of the gamma ray interaction in the crystal are determined from a maximum likelihood calculation. The depth of an interaction in the crystal is inferred

from the width of the light distribution. Accurate depth determination eliminates parallax errors and could provide an ultimate spatial resolution of 4.5 mm.

A current area of development is "time of flight" PET (Ter-Pogossian et al., 1981). By noting the difference in arrival times of two coincident gammas the common site of origin can be localized along the line determined by the two detection sites (Fig. 10). For this application, a very short scintillation decay time is paramount, suggesting use of cesium or barium fluoride. Coincidence resolving times of 3×10^{-10} seconds have been achieved with CSF. Since photons travel at 3×10^{10} cm/sec this allows a positron uncertainty along the event line of about 4.5 cm FWHM. Since spatial resolution of the order of 1 cm is achieved with comparable geometry but without time of flight, the main consequence is an improvement in signal to noise in the final image.

Plastic scintillators are attractive because they are inexpensive, easily fabricated, and fast. They are used in a novel 8-ring design with 1024 detectors per ring, each detector 2.4 mm wide to provide high spatial resolution (McIntyre, Spross, and Wang, 1986). The number of photomultiplier tubes per ring is only 72. This economy is achieved by the use of optical fibers in an address-coding scheme where each detector element is connected to a number of tubes, to provide radial, azimuthal and axial location of each event. Plastic scintillators have low intrinsic efficiency since their density and effective atomic number are both low, and the great radial extent required to achieve practical sensitivity necessitates radial address in each ring to avoid parallax errors.

A coding scheme was used in an early planar system, the MGH Positron Camera (Brownell et al., 1972). Each planar detector consisted of an array of 127 NaI crystals 20 mm diameter, 38 mm long. Each of 72 phototubes viewed part of four different crystals (Fig. 11). This coding simplified the coincidence logic and reduced the cost of photomultiplier tubes and associated circuitry.

Crystal scintillators are not the only materials used for positron detectors. High Density Avalanche Chambers (HIDAC) have high Z metal structures (Pb,W) which have high efficiency for photo electric interactions, but are porous enough to allow the photo electron to escape to a channel through the metal (Fig. 12). In a channel the photo electron produces secondary electrons by ionization of a gas, and the secondary electrons are accelerated by an electric field, producing electron gain. This jet of ionization electrons is directed to a multiwire proportional chamber which can efficiently measure the coordinates of the electron jet, and provide a signal to establish coincidence in a diametrically opposed HIDAC detector. The converters may be layers of lead foil, separated by insulation, pierced by a close-packed array of holes by a computer-controlled machine tool, and with the successive layers electrically connected to a resistive divider which supplies the accelerating voltage (Jeavons et al., 1981). An alternate converter structure (Lanza et al., 1986) is a mesh of tungsten wires with successive layers at higher electrical potentials. The wire diameter and pitch are chosen to optimize the conflicting probabilities of high photon interaction, and high electron escape. A third geometry uses close packed lead glass tubing with a resistive surface (Fujieda et al., 1986). The presence of an electrical potential difference along the tube accelerates the ionization electrons, produced by a primary photo electron escaping from the tubing wall, providing electron gain.

The intrinsic efficiency for annihilation photons in a single HIDAC detector is only a few percent, small compared to that for typical scintillator systems, and

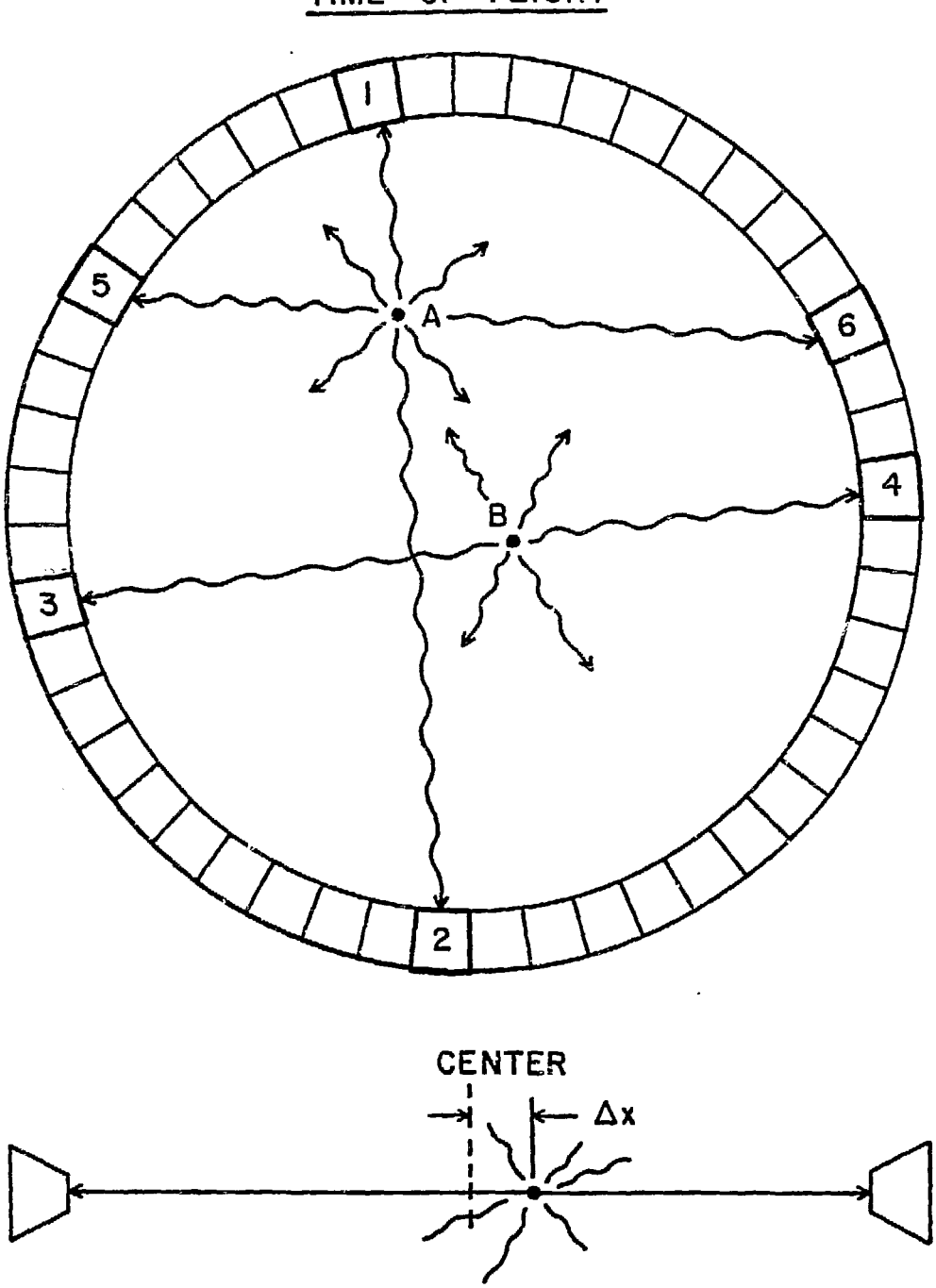

Fig. 10. Time-of-flight PET uses the difference in arrival time of the annihilation photons to limit the region along the event line where the annihilation occurred.

abysmal when one notes that the positron detection efficiency is the square of the singles efficiency. However, a stack of detectors may be placed on each side with the net intrinsic efficiency equal to the sum of those for each unit. Each detector assembly

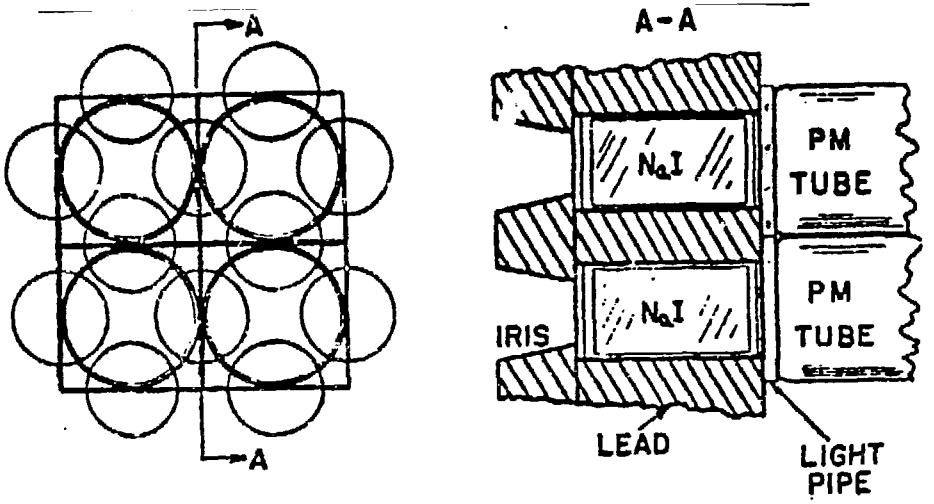

Fig. 11. Coding technique used in the MGH positron camera to couple the crystals to the phototubes in the detector.

is only a few cm thick but successive elements will be further from the test object and thus have reduced geometric efficiency. In addition, the reconstruction algorithm employed demands spatial invariance, limiting the angle between an event line and the detector to detector centerline, producing a further reduction in geometric efficiency.

The advantages of the HIDAC approach include extremely good spatial resolution, 2 mm FWHM intrinsic (Fig. 13), low materials cost, a relatively robust structure without the sensitivity to mechanical and thermal shock characteristic of crystals, and intrinsically digital output, i.e. the wires impose discrete addressing.

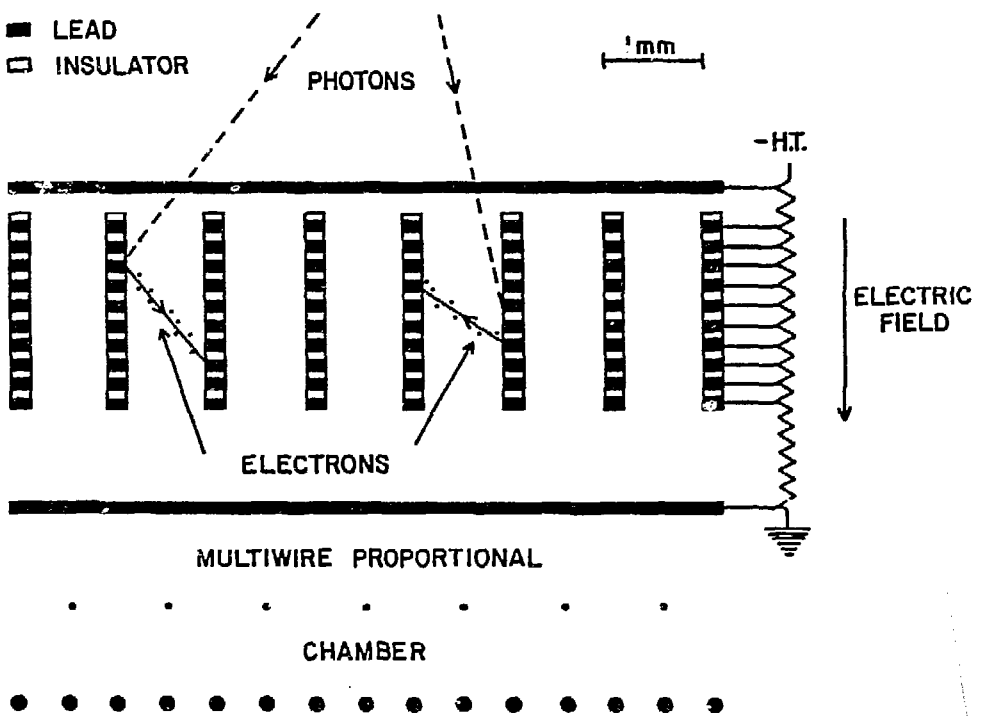

Fig. 12. The HIDAC detector consists of a convector section where gamma rays produce electrons which are amplified and accelerated into a multi-wire chamber which gives their location in space and time (Jeavons et al., 1981).

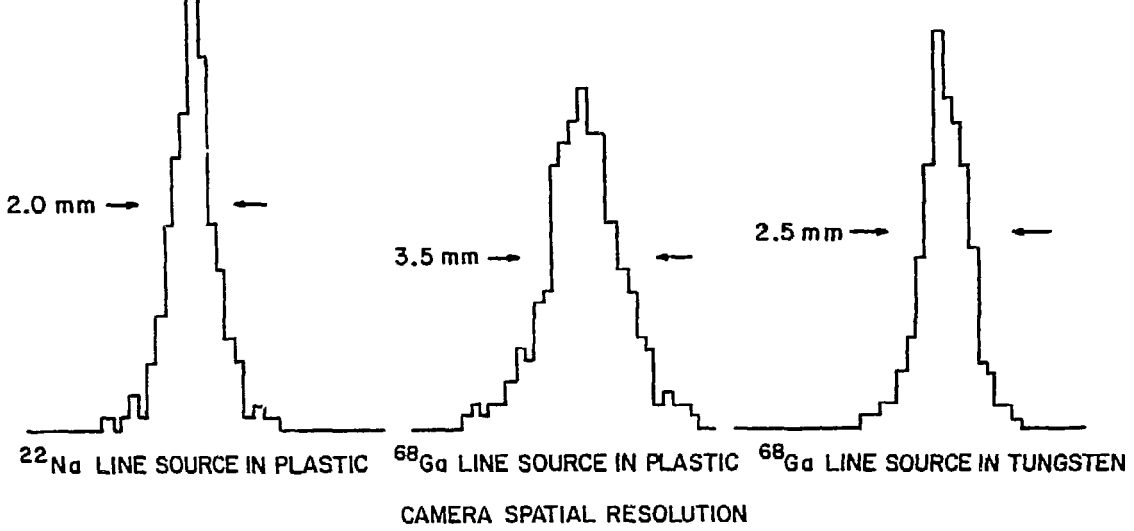

Fig. 13. Spatial resolution measured with a HIDAC camera. ^{68}Ga emits positrons with higher energy than ^{22}Na. This increased range effect is minimized by replacing the plastic with tungsten (from Jeavons et al., 1981).

The case for high spatial resolution is made (Phelps et al., 1982) in Fig. 14, showing the modulation transfer function (MTF) for systems with various intrinsic resolutions. MTF is the image (perceived) contrast for an object contrast of 100% (alternating hot and cold object structure). Here contrast is

$$C = \frac{I_{hot} - I_{cold}}{I_{hot} + I_{cold}}$$

where I is the image event density in the hot or cold areas of the object. For the 12 mm resolution system structures with spatial frequencies greater than .08 mm^{-1}, corresponding to a 12.5 mm wavelength, have an image contrast of only 5%, requiring a large number of counts to resolve an object with this spatial frequency when one considers the effect of statistical noise. The system with 2 mm resolution has only an 8% loss in image contrast at the same frequency, thus requiring far fewer counts for the same noise equivalence.

Quantitation

Ideally, emission tomography supplies the investigator with accurate maps of the quantitative distribution *in vivo* of the radionuclide injected. This requires an appreciation of the myriad processes which cause the measured distribution to deviate quantitatively and qualitatively from the true distribution. The variety of effects causing this deviation, absorption, scattering, "accidentals" are illustrated in Figure 15. Accurate *attenuation correction requires* a knowledge of the distribution of the attenuation coefficient throughout the volume of interest. This distribution may be obtained by performing a transmission scan of the subject before injecting the radionuclide. An external ring or sheet source is imaged alone, then data is taken with the external source and subject in place. The attenuation correction for each ray is the ratio of event rate for that ray for the source alone relative to the event rate for subject and source. The external source is then removed and the emission study can commence. The corrected image is obtained by multiplying the emission rate in each ray or channel by the ratio of target alone to target plus subject from the transmission study.

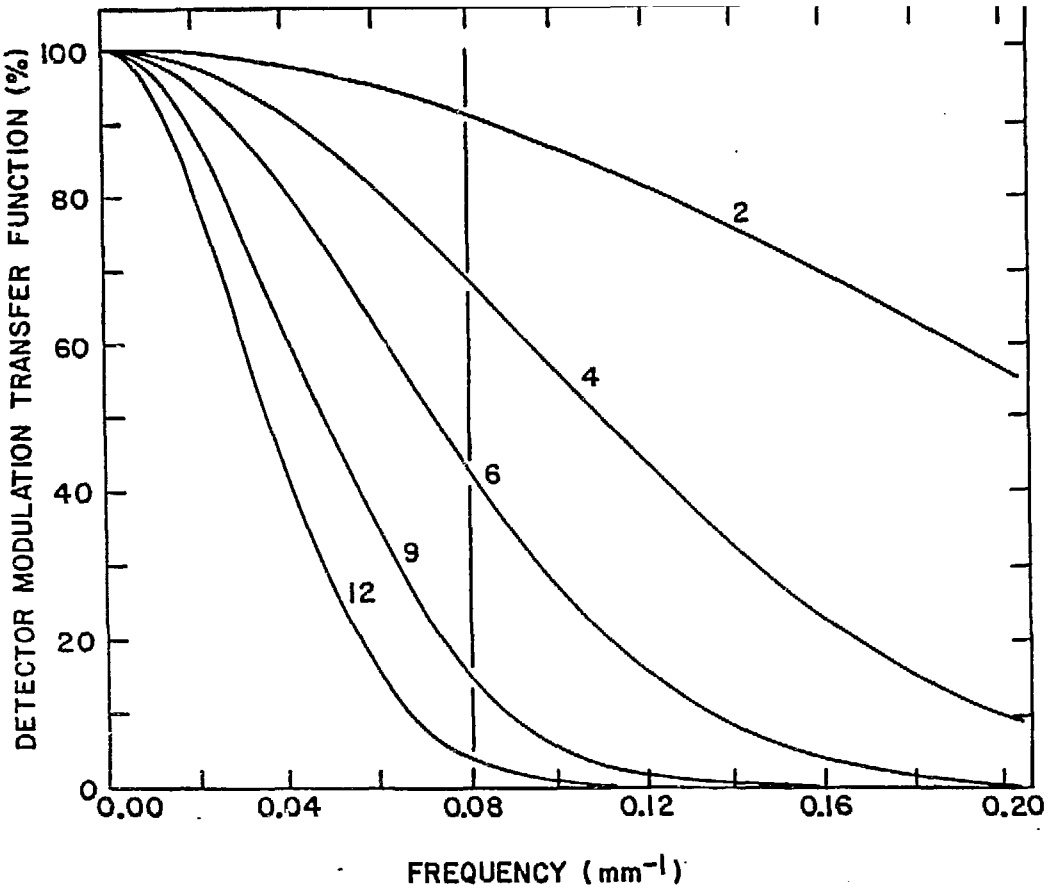

Fig. 14. Modulation transfer functions vs spatial frequency for detectors with spatial resolution indicated. Vertical line shows conventional cutoff frequency for a ramp reconstruction filter to produce an image resolution slightly worse that that from the detector of 12 mm FWHM. Note amplification of frequencies upto this cutoff as detector resolution is improved.

The practical difficulties arising from this approach include increased procedure time, increased patient dose, increased statistical noise, and repositioning artifacts due to different positions of the subject for the two phases of the process. The last problem is often unavoidable if the time from injection to start of emission imaging is longer than a small fraction of an hour; some radiopharmaceuticals, for example, require of the order of an hour to equilibrate in the organ of interest, and to wash out of surrounding tissue and improve contrast.

An alternate approach is to determine the surface contour of the patient for the volume of interest, or more practically, to choose an ellipse "equivalent" to the surface contour and assume a uniform attenuation distribution within that contour. This approach eliminates the need for a transmission scan of good statistics. Often the emission image is sufficient to allow fitting of the surface ellipse, or a preliminary transmission scan can be used for that purpose. Obviously, the problem of registration between the true attenuation distribution and that used for the attenuation correction is compounded further by these assumptions.

Little use has been made to date of the attenuation information from transmission x-ray (CAT) scans due to the problem of scaling dimensions from one instrument to the other. The problem of registration is magnified by uncertainty in the axial as well

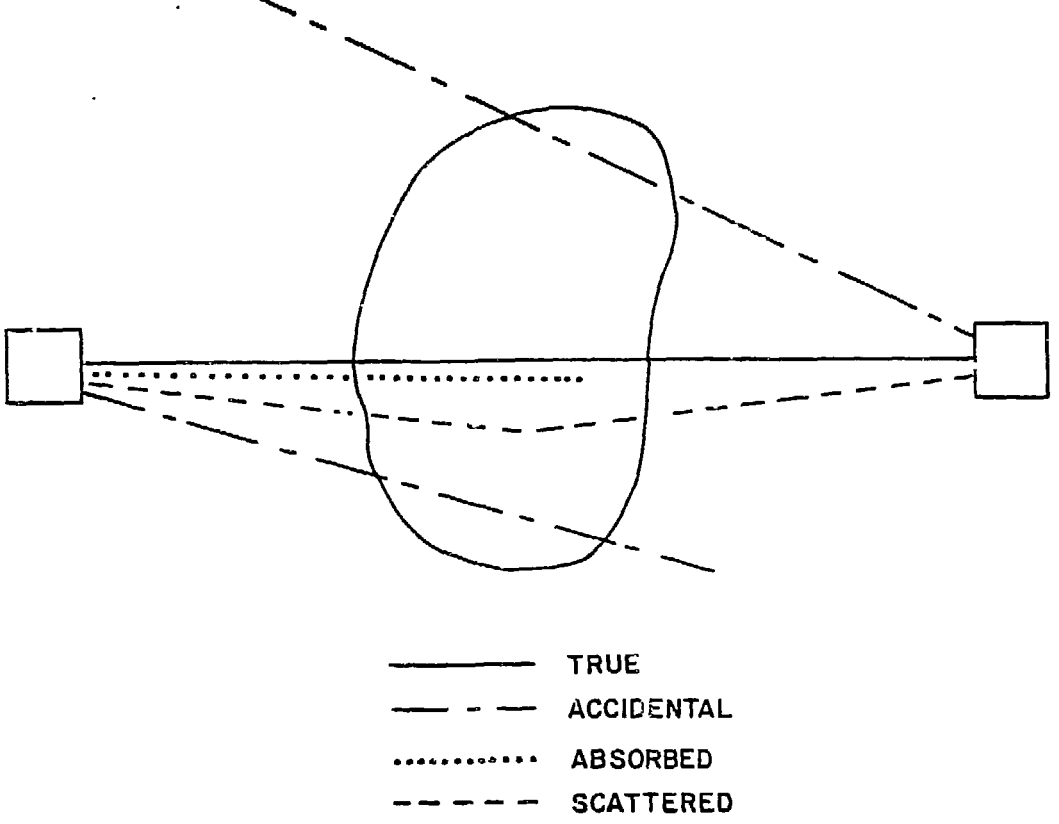

Fig. 15. The processes which distort quantitation in positron emission tomography.

as the lateral dimensions, and to these must be added the problem of correcting the attenuation data from the (broad) energy of the CAT x-ray source to annihilation energy.

Attenuation reflects the two processes – absorption and scattering. The number and degree of scattered events included in the image is determined by the geometry and the spectral response of the detector system. Lowering the threshold energy of the scintillation detectors increases the observed event rate, but at the price of accepting more photons which have scattered in the body. Similarly, increasing the separation of the detectors improves scatter rejection (Atkins, 1978).

Random coincidences occur when photons from the annihilation of separate positrons generate signals within an interval less than the coincidence time "window." Correction for accidental or random coincidences also poses problems of statistical noise and positioning just as in attenuation correction. The magnitude of the random counts included in the total observed events may be estimated from the apparent event density beyond the object's boundary, or measured by a delayed coincidence circuit, or calculated from the singles rates knowing the coincidence resolving time. The delayed coincidence circuit has a delay, much greater than the resolving time, inserted in the circuit path on one side. The prompt coincidence circuit generates pulses for true and accidental events, the delayed circuit signals only the random events; the difference reflects the number of true coincident events.

The shape of the accidentals distribution is also required to make a correction to the distribuition. A low order approximation is that the accidentals are uniformly

distributed. This is a workable premise if the randoms are a small fraction of the total events. In practice, the accidentals distribution is not uniform but is quite "broad;" i.e., it exhibits little high spatial frequency structure and is highly symmetric. The randoms distribution may be mapped for a test source by triggering the event position recording process only via delayed coincidences, or by imaging the distribution of a single photon emitting nuclide with appropriate energy. The single gamma emitting isotope most commonly used for this purpose is Strontium-85 (E_γ – 514 KeV, intensity = .933, $T_{1/2}$ = 64.8 days).

The primary step in PET quantitation is imaging a known distribution representative of the clinical application. A head imaging instrument is typically run each day with a cylindrical phantom containing known concentrations of Ga-68/Ge-68 in equilibrium in aqueous solutions in four or five compartments. A reconstruction of this distribution, corrected for absorption and other processes, gives a conversion scale from detected events per unit volume to activity per unit volume. This procedure also serves as a final quality assurance check on the system, when the results are compared with preceding values.

SUMMARY

Positron-emitting radionuclides permit the use of electronic collimation and thus achieve higher resolution and better sensitivity than can be obtained with gamma-emitting radiotracers. The evolution of PET imaging systems can be traced from the use of opposed collimated scanning detectors, which had all the limitations of traditional single photon imaging devices, to the present systems which surround the subject with a large volume of detector material. The improvements in system resolution now approach the theoretical limitation imposed by positron-range, and angular deviation. The use of coding permits the use of shared electronics for reading out multiple detectors, which promises to decrease the cost of PET imaging devices, at some penalty of degraded performance. Improvements in computer architectures and capabilities permit faster reconstruction of the multiple planes imaged by multi-slice imaging systems. Software for distortion correction and image processing are still under development, and the ability to map between different devices requires the coordination of efforts between different groups in the same institution. The development and validation of the mathematical models for tracer kinetic analyses will continue to occupy the attention of clinicians and scientists involved in these developments. The desire to make these devices simple and cheap enough to be used in routine patient care is occupying the attention of industry and pioneering users, but this goal has not yet been achieved.

REFERENCES

Aronow, S. 1962, Positron Brain Scanning, in: "Progress in Medical Radionuclide Scanning," R. Kniseley, G. Andrews, and C. Harris, ed., Oak Ridge Inst. of Nuclear Studies, Oak Ridge Tennessee.

Atkins, F. 1978 "Monte Carlo analysis of photon scattering in radionuclide imaging," thesis, Univ. of Chicago.

Brownell, G., Burnham, C., Hoop, B., and Kazemi, H., 1972, Positron Scintigraphy with Short-lived Cyclotron Produced Radiopharmaceuticals and a Multicrystal Positron Camera, in: "Medical Radioisotope Scintigraphy", IAEA, Vienna.

Budinger, T. 1978 "A primer on reconstruction algorithms," Lawrence Berkeley Laboratory Report LBL-8212.

Burnham, C., Bradshaw, J., Kaufman, D., Chester, D., Stearns, C., and Brownell, G., 1982 Application of a one dimensional scintillation camera in a positron ring detector, IEEE Trans. Nucl. Sci. NS-29:461.

Derenzo, S., Budinger, T., Huesman, T., Calsoon, J., and Vuletich, T. (1981) Imaging properties of a positron tomograph with 280 BGO crystals, IEEE Trans Nuc. Sci. NS-28:81.

Evans, Robley D. The atomic nucleus, McGraw Hill, New York 1955, p. 538.

Fujieda, I., Mulera, T., Perez-Mendez, V., and Del Guerra, A., 1986 "Further measurements of electron transmission and avalanche gain in narrow lead glass tubing IEEE Trans. Nuc. Sci. 33:587.

Iida, H., Kanno, I., Miura, M., Murakami, M., Takahashi, K., and Vemura, K. 1986 A simulation study of a method to reduce positron annihilation spread distribution using a strong magnetic field in positron emission tomgraphy, IEEE Trans. Nucl. Sci. NS33:597.

Jeavons, A., Schorr, B., Kull, K., Townsend, D., Frey, P., and Donath, A. 1981 A large area stationary positron camera using wire chambers in "Medical Radionuclide Imaging 1980" IAEA, Vienna.

Karp, J., Muehllehner, G., Beerbohm, D., and Markoff, D., 1986, Event localization in a continuous scintillation detector using digital processing, IEEE Trans. Nuc Sci, NS-33: 550.

Lanza, R.C., Osborne, L.S., Holman, B.L., and Zimmerman, R.E., 1986, Mesh chambers for positron emission tomography, IEEE Trans Nuc Sci, NS-33: 482.

McIntyre, J.A., Spross, R.L., and Wang, K.H., 1986, Construction of a positron emission tomograph with 2.4 mm detectors, IEEE Trans Nuc Sci, NS-33: 425.

Phelps, M., Huang, S., Hoffman, E., Plummer, D., and Carson, R. 1982 An analysis of signal amplification using small detectors in positron emission tomography J. Comp Ass Tomo, 6:551.

Ter-Pogosian, M. Physical aspects of emission computed tomography, in Radiology of the skull and brain, vol. 5, Newton, T., and Potts, D., ed. C. V. Mosbry Co. St. Louis 1981.

Ter-Pogossian, M., Mullani, N., Ficke, D., Markham, J., and Snyder, D. 1981 Photon time-of-flight assisted positron emission tomography J. Comp. Ass. Tomo. 5:227.

Yano, Y., 1986 "Essentials of a Rubidium-82 generator for nuclear medicine," Lawrence Berkeley Laboratory Report LBL-21810.

ACKNOWLEDGMENTS

The submitted manuscript has been authored under Contract No. DE-AC02-76CH00016 with the U.S. Department of Energy.